Structures and gating mechanism of human TRPM2

Longfei Wang[1,2,*], **Tian-Min Fu**[1,2,*,†], **Yiming Zhou**[3,4], **Shiyu Xia**[1,2], **Anna Greka**[3,4], and **Hao Wu**[1,2,†]

[1]Department of Biological Chemistry and Molecular Pharmacology, Harvard Medical School, Boston, MA 02115, USA.

[2]Program in Cellular and Molecular Medicine, Boston Children's Hospital, Boston, MA 02115, USA.

[3]Department of Medicine, Brigham and Women's Hospital and Harvard Medical School, Boston, MA 02115, USA.

[4]Broad Institute of MIT and Harvard, Cambridge, MA 02142, USA.

Abstract

Transient receptor potential (TRP) melastatin 2 (TRPM2) is a cation channel associated with numerous diseases. It has a C-terminal NUDT9 homology (NUDT9H) domain responsible for binding adenosine diphosphate (ADP)–ribose (ADPR), and both ADPR and calcium (Ca^{2+}) are required for TRPM2 activation. Here we report cryo–electron microscopy structures of human TRPM2 alone, with ADPR, and with ADPR and Ca^{2+}. NUDT9H forms both intra- and intersubunit interactions with the N-terminal TRPM homology region (MHR1/2/3) in the apo state but undergoes conformational changes upon ADPR binding, resulting in rotation of MHR1/2 and disruption of the intersubunit interaction. The binding of Ca^{2+} further engages transmembrane helices and the conserved TRP helix to cause conformational changes at the MHR arm and the lower gating pore to potentiate channel opening. These findings explain the molecular mechanism of concerted TRPM2 gating by ADPR and Ca^{2+} and provide insights into the gating mechanism of other TRP channels.

†Corresponding author. tianmin.fu@childrens.harvard.edu (T.-M.F.); wu@crystal.harvard.edu (H.W.).
*These authors contributed equally to this work.

SUPPLEMENTARY MATERIALS

www.sciencemag.org/content/362/6421/eaav4809/suppl/DC1

Materials and Methods
Figs. S1 to S12
Table S1
References (39–51)

Graphical Abstract

INTRODUCTION: Transient receptor potential (TRP) melastatin 2 (TRPM2) is a Ca^{2+}-permeable, nonselective cation channel implicated in the development of many inflammatory and neurodegenerative diseases. Human TRPM2 has a C-terminal NUDT9H domain, which shares similarity to the NUDT9 enzyme that hydrolyzes adenosine diphosphate (ADP)–ribose (ADPR). Previous studies showed that TRPM2 is co-activated by ADPR and Ca^{2+}. However, the molecular mechanism of human TRPM2 activation remains elusive.

RATIONALE: To address the gating mechanism of human TRPM2, we aimed to resolve the structures of full-length human TRPM2 in different states. By optimizing expression and purification procedures, we obtained homogeneous recombinant TRPM2 samples from human embryonic kidney (HEK) 293F cells. With single-particle cryo–electron microscopy (cryo-EM), the structures of human TRPM2 alone, in complex with ADPR, and in complex with ADPR and Ca^{2+} were determined to 3.6-,6.1-, and 6.4-Å resolution, respectively.

RESULTS: Human TRPM2 assembles into a tetramer with a three-tier architecture, which resembles other structures in the TRPM family (see the figure). The bottom tier is composed of the C-terminal NUDT9H domain, the N-terminal MHR1/2 and MHR3 domains, and the pole helix. The middle tier consists of the MHR4 domain and the rib helix, whereas the top tier comprises the S1 to S6 transmembrane helices and the TRP helices, including TRP H1.

One notable feature in the human TRPM2 apo structure is that the NUDT9H domain, which is responsible for sensing ADPR, as shown by binding affinity measurements, folds back to form extensive interactions with the TRPM2 N-terminal domains both in cis and in trans. Upon ADPR binding, the NUDT9H domain and the MHR1/2 domain undergo a 27° rigid-body rotation, which disrupts the trans interaction between NUDT9H and MHR and may prime the channel for opening. Compared with the ADPR-bound structure, the ADPR and Ca^{2+}–doubly bound TRPM2 undergoes a 15°rotation in the cytoplasmic domain, a tilt of the TRP helix, and a twist of the S6 gating helix to open the channel. The structures collectively provide a full depiction for the mechanism of human TRPM2 activation (see the figure).

In addition, our structures highlight several differences in the gating mechanism of TRPM2 across species. In contrast with our observation that the NUDT9H domain of human TRPM2 is required for channel coactivation by ADPR and Ca^{2+}, the open-state structure of zebrafish TRPM2 revealed an unexpected ADPR-binding site at the MHR1/2 domains. To resolve this inconsistency, we demonstrated that NUDT9H of human TRPM2 has a substantially higher affinity to ADPR than that of zebrafish TRPM2, and that mutation of MHR1/2 residues in human TRPM2 equivalent to the ADPR-binding residues in zebrafish TRPM2 does not compromise human TRPM2 channel opening. A second major difference is that the P loop of NUDT9H responsible for the trans interaction in human TRPM2 is absent in NUDT9H of zebra-fish TRPM2, which does not closely associate with the MHR arm in the apo state. Moreover, in comparison with sea anemone TRPM2, in which the NUDT9H domain hydrolyzes ADPR but does not contribute to channel opening, NUDT9H of human TRPM2 binds ADPR to promote channel opening but does not degrade ADPR. Together, these species-specific features reflect functional and mechanistic complexity in TRPM2 and the TRP superfamily during evolution.

CONCLUSION: Structures of human TRPM2 alone, in complex with ADPR, and in complex with ADPR and Ca^{2+} elucidate the mechanism of TRPM2 gating and provide a framework for the understanding of TRPM2-associated diseases. Although it is conserved across species that TRPM2 is coactivated by ADPR and Ca^{2+}, the organization of the NUDT9H domain and how the orthologs respond to ADPR seem to diverge on the basis of our and previously resolved structures of TRPM2. Moreover, our structures reveal an important role of the TRP helix in TRPM2 gating, which may be universal in many other TRP channels.

—
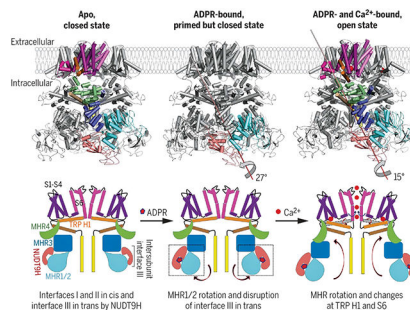
Activation mechanism of the human TRPM2 channel. Cryo-EM structures of full-length human TRPM2 in apo (closed), ADPR-bound (closed), and ADPR- and Ca^{2+}-bound (open) states and corresponding cartoons that illustrate the gating process of the channel.

The transient receptor potential melastatin (TRPM) family belongs to the superfamily of transient receptor potential (TRP) ion channels and is involved in multiple biological processes and diseases (1–3). In humans, there are eight TRPMs, which share sequence similarity but respond to different stimuli (1–3). TRPM family members share a core architecture that includes a large TRPM homology region (MHR1 to 4), a six-helix trans-membrane (TM) domain, a conserved TRP helix region, a rib helix, and a pole helix (Fig. 1A). In addition to the core, some TRPMs have an additional enzyme domain that regulates gating and are sometimes classified as chanzymes (1). For example, TRPM2 has a C-terminal NUDT9 homology (NUDT9H) domain, which has a predicted fold belonging to the Nudix hydrolase family that catalyzes the conversion of adenosine diphosphate (ADP)–ribose (ADPR) to adenosine monophosphate (AMP) and ribose-5-phosphate (R5P). It has been debated whether the NUDT9H domain of TRPM2 has enzymatic activity (4, 5).

TRPM2 forms a Ca^{2+}-permeable nonselective cation channel gated by ADPR and Ca^{2+} (6–9). ADPR is a metabolic product of nicotinamide adenine dinucleotide (NAD) and accumulates in cells upon oxidative stress. TRPM2 relays oxidative stress to Ca^{2+} signaling with many vital physiological roles (10–13). In particular, TRPM2 plays prominent functions in immunity and inflammation, which include chemokine production, inflammasome activation, and infection control (8, 14–18). Under pathological conditions such as ischemia-reperfusion injury, inflammation, and Alzheimer's disease, TRPM2 can be activated by high levels of reactive oxygen species through ADPR accumulation and exacerbates the diseases (19, 20). Therefore, TRPM2 is an attractive therapeutic target against chronic inflammatory and neurodegenerative diseases.

Recently reported cryo–electron microscopy (cryo-EM) structures of human TRPM4 (21–24), *Ficedula albicollis* TRPM8 (25), *Nematostella vectensis* TRPM2 (*nv*TRPM2) (26), and mouse TRPM7 (27) have shed light on the closed, inactive core architecture of TRPM family cation channels. Here we determined the cryo-EM structures of full-length human (*Homo sapiens*) TRPM2 (*hs*TRPM2) in apo, ADPR-bound, and ADPR- and Ca^{2+}-bound states. Instead of being flexibly linked to the C-terminal end as previously presumed (26), NUDT9H folds back onto the N-terminal domain to form extensive interactions with MHR through both intra- and intersubunit contacts. Upon ADPR binding, NUDT9H undergoes conformational changes that trigger the rotation of MHR1/2 and dislodging of the intersubunit interaction. This ADPR-induced "priming" effect may further allow Ca^{2+} binding to concertedly tilt the TRP helix, twist the MHR, and rotate the gating S6 helix to open the channel. Unexpectedly, the cryo-EM structure of zebrafish (*Danio rerio*) TRPM2 (*dr*TRPM2) in complex with ADPR and Ca^{2+} published recently shows ADPR binding at the MHR1/2 region (28). Our further experimental evidence confirmed the species-specific difference in ADPR binding and gating using NUDT9H for *hs*TRPM2 and MHR1/2 for *dr*TRPM2, respectively.

Structure of full-length *hs*TRPM2 in the apo state

We expressed *hs*TRPM2 in human embryonic kidney (HEK) 293F cells and purified it in the absence of ADPR and Ca^{2+} (fig. S1). We then determined its fourfold symmetric cryo-EM structure at 3.6-Å resolution (figs. S2 and S3, and table S1). The initial cryo-EM density map was of sufficient quality for modeling the N-terminal cytosolic domains but not NUDT9H and the TM region. Using density subtraction and focused three-dimensional (3D) classification followed by local refinement, we improved the cryo-EM maps at these regions (figs. S2 and S3). The final map revealed a square-shaped structure with approximate dimensions of 150 Å by 100 Å by 100 Å, and the final model comprises all domains except the linker between the pole helix and the NUDT9H domain (Fig. 1, A and B).

The overall structure of *hs*TRPM2 is similar to that of *dr*TRPM2 (28) (fig. S4A), with NUDT9H prominently decorating the bottom corners of the large intracellular region of the tetramer (Fig. 1, B and C). In a three-tier description of the overall architecture that has been used for TRPM channels, NUDT9H resides on the bottom tier, which also comprises the N-terminal MHR1/2, MHR3, and the pole helix (Fig. 1, C to E). Surrounded by MHR1/2, the symmetric pole helices form a parallel tetrameric coiled coil at the fourfold axis. The middle tier of TRPM2 consists of the rib helix and the MHR4 domain; the latter provides stacked α helices to bridge the N-terminal cytosolic domain and the TM region. We call the entire MHR region the MHR arm (Fig. 1A). The top tier is composed of pre-S1, S1 to S6 TM domain helices, and the TRP helices. As in most classic six-pass cation channels, the TM region of TRPM2 is arranged in a domain-swapped architecture, where the S1-S4 voltage sensing–like domain (VSLD) of one subunit interacts with the S5-S6 pore domain of a neighboring subunit (fig. S4, B and C).

Cis and trans interactions between NUDT9H and MHRs

NUDT9H adopts a two-domain architecture, in which the N-terminal domain (NTD) is dominated by loops and short β strands, and the C-terminal domain (CTD) comprises a central β sheet surrounded by several α helices (Fig. 2A). NUDT9H resembles human NUDT9 (29), a mitochondrial ADPR pyrophosphatase, and has a conserved P loop that connects two b strands in the central β sheet of the NUDT9H CTD (Fig. 2, A and B). NUDT9H lies adjacent to MHR1/2 and MHR3 in the same subunit and also interacts with MHR1/2 of a neighboring subunit. We defined three contact areas: interfaces I, II, and III (Fig. 2C). Interfaces I and II mediate intrasubunit (cis) interactions of NUDT9H with MHR1/2 and MHR3, respectively (Fig. 2, D and E). Interface III enables intersubunit (trans) interactions between the P loop of NUDT9H in one subunit and MHR1/2 of a neighboring subunit (Fig. 2F). Through these interfaces, NUDT9H couples neighboring subunits by occupying the groove between two MHR arms, thereby restricting intersubunit movement and likely stabilizing the MHR arms in the absence of ADPR binding (Fig. 2C). Of note, despite the overall similarity in the subunit structure, this inter-subunit interaction is absent in *dr*TRPM2 (fig. S4D), likely owing to the P-loop deletion in *dr*TRPM2 NUDT9H (fig. S4, E and F).

MHR1/2 rotation, MHR3 allosteric change, and dislodging of the intersubunit interface upon ADPR binding

To obtain a structure of TRPM2 in complex with ADPR, we first showed by surface plasmon resonance that the NUDT9H domain of *hs*TRPM2 directly interacts with ADPR with a measured affinity of ~15 mM (Fig. 3A), similar to the measured affinity of ~41 mM for ADPR binding to full-length *hs*TRPM2 (Fig. 3A) (7, 30–32). The NUDT9H domain is also absolutely required for channel gating (fig. S5, A to C), and TRPM2 does not hydrolyze ADPR (4, 5) (fig. S5, D and E). By contrast, the *dr*TRPM2 structure revealed functionally important ADPR binding at the MHR1/2 domain (28). To determine whether the ADPR-binding site at MHR1/2 is also important for *hs*TRPM2, we generated the double mutant R302A/R358A ($Arg^{302} \rightarrow Ala/Arg^{358} \rightarrow Ala$), whose equivalent in *dr*TRPM2 nearly abolished ADPR-induced current (28). We found by Ca^{2+} imaging that the mutant did not substantially affect channel gating by ADPR (fig. S5, B and C), suggesting that the ADPR-binding site observed in *dr*TRPM2 does not play an important role in *hs*TRPM2. We further expressed the NUDT9H domain of *dr*TRPM2 and found that its binding affinity to ADPR is close to millimolar, much reduced in comparison to the NUDT9H domain of *hs*TRPM2 (fig. S5, F and G), which is also consistent with the multiple mutations in *dr*TRPM2 at the proposed NUDT9H ADPR-binding site (30) (fig. S4F). These data collectively demonstrate that *dr*TRPM2 and *hs*TRPM2 use MHR1/2 and NUDT9H domains, respectively, for ADPR sensing.

We then purified TRPM2 in the presence of ADPR and EDTA to chelate Ca^{2+} and obtained a cryo-EM density map at 6.1-Å resolution (fig. S6 and table S1). Despite the limited resolution of this state, a comparison to the apo state reveals dramatic conformational changes at the bottom tier where NUDT9H, MHR1/2, and MHR3 reside (Fig. 3, B and C).

In particular, interface III between NUDT9H of one subunit and the MHR1/2 domain of a neighboring subunit is lost upon ADPR engagement (Fig. 3B). MHR1/2 rotates about 27° toward NUDT9H, clockwise if viewed from the extracellular side, whereas the remainder of the TRPM2 subunit structure does not show large changes (Fig. 3, C to E). Although the change at the MHR1/2 region is mostly rigid-body movement (fig. S7A), the MHR3 region, especially the helical hairpin that interacts with the NUDT9H CTD on one side and MHR1/2 on the other side, exhibits substantial local conformational changes (fig. S7B).

To deduce conformational changes at NUDT9H upon ADPR binding, we fit the apo NUDT9H model as a rigid body into the cryo-EM density of the ADPR-bound form (Fig. 3F). In the homologous NUDT9 crystal structure [Protein Data Bank (PDB) 1QVJ], the hydrolytic product R5P sits in a cleft between the NTD and CTD (29), and docking, molecular dynamics simulation, and mutagenesis identified the crevice between the NTD and CTD as an ADPR-binding site (30). We could not resolve the bound ADPR in our density but observed that the NTD-CTD crevice is smaller, consistent with direct ADPR binding (Fig. 3F). The density also suggests that the NTD needs to rotate relative to the CTD to fit better, likely leading to changes at the interface with MHRs. In addition, the P-loop region is considerably different, which may contribute to the disengagement of interface III between NUDT9H and MHR1/2 in trans. NUDT9H is likely bifunctional: It inhibits MHR movement in the absence of ADPR through intra- and intersubunit interactions and induces MHR rotation and dislodging of the intersubunit interaction in the presence of ADPR. As discussed below, these changes collectively "prime" TRPM2 for channel opening by Ca^{2+} binding, and we therefore named the ADPR-bound state the primed state.

Global conformational changes upon coactivation by ADPR and Ca^{2+}

It has been shown that although ADPR is required for TRPM2 opening, the channel remains closed until Ca^{2+} binds at the TM region (9). Using single-channel recording, we recapitulated the process of channel opening synergistically triggered by ADPR and Ca^{2+} (fig. S8). To elucidate coactivation by ADPR and Ca^{2+}, we purified *hs*TRPM2 in the presence of ADPR and Ca^{2+} and obtained a cryo-EM map at 6.4-Å resolution (fig. S9 and table S1). Although the structure is only at a modest resolution, the global organization of the domains and the TM helices are well defined. In contrast to the clockwise rotation between the ADPR-bound state and the apo state (Fig. 3D), subunits in the open-state structure undergo counterclockwise rotation in comparison with the ADPR-bound state when viewed from outside the cell (Fig. 4, A and B). The subunit structure in the primed state is similar to that in the open state, suggesting that the rotation is largely rigid body in nature (Fig. 4C). Whereas the rotation from apo to primed involves mostly the bottom MHR arm, the rotation from primed to open involves both the middle and bottom tiers, as well as conformational adjustments in the TM region (Fig. 4A).

The Ca^{2+}-binding site is localized near the intracellular border of the channel, in between S2, S3, and the TRP H1 helix. Despite the modest resolution, the electron density was best interpreted as Ca^{2+} being coordinated by res idues E843 and Q846 of S2, N869 of S3 and E1073 of TRP H1 (E, Glu; Q, Gln; and N, Asn) (Fig. 4D and fig. S10A). Involvement of the TRP helix in Ca^{2+} coordination has not been observed in structures of other TRP channels

but is consistent with the coordination seen in the higher resolution *dr*TRPM2 structure (PDB 6DRJ) even though the authors did not point this out (28) (Fig. 4D). In the *nv*TRPM2 structure in the absence of ADPR, the TRP H1 residue equivalent to E1073 locates right below the observed Ca^{2+} site (fig. S10B), and mutagenesis on this residue also compromised Ca^{2+} sensitivity as it did on residues on S2 and S3 (26). Notably, E1073 of TRP H1 is highly conserved in different TRPM channels (fig. S10C). These data support a subtle, but notable, difference in Ca^{2+} coordination in the presence and absence of ADPR.

Binding of Ca^{2+} is associated with a tilt at TRP H1, which, in turn, is intimately associated with the cytosolic domain through its interaction with MHR4 using extensive hydrophobic and hydrogen-bonding interactions (Fig. 4E). We propose that this TRP-MHR coupling is responsible for the transmission of the Ca^{2+}-binding signal to the cytosolic domain. Superposition of just the TRP-MHR4 region between the closed and open states suggests that the coupling is mostly rigid body (fig. S10D). Because of the large dimensions of the MHR arm, a subtle conformational change at TRP H1 may be amplified to large movement at the bottom tier of the structure (Fig. 4A). We propose that neither Ca^{2+} binding nor ADPR binding alone provides a sufficient amount of energy to elicit the concerted conformational changes that involve MHR1/2 rotation, local changes at MHR3, and global rotation of the entire cytosolic domain. Instead, two binding events likely mutually prime each other to share the energetic cost required for the conformational changes. For *hs*TRPM2, these conformational changes may also be restricted by the intersubunit interaction exerted through the NUDT9H domain (Fig. 2C). Freeing the subunits from this intersubunit restriction through ADPR binding may then also facilitate any conformational changes required for regulation and gating.

Conformational changes at the pore region associated with TRPM2 channel gating

As in other TRP channels, the ion permeation pathway in TRPM2 is composed of a selectivity filter, a central cavity, and a lower gate (Fig. 5, A to D). The selectivity filter and the central cavity of TRPM2 are relatively invariant among the different states (Fig. 5, A to C). The lower gate, however, is highly restricted in the apo and primed states, with I1045 (I, Ile) of S6 forming the most constricted point to block ion flow (Fig. 5, A, B, and D). In the state doubly bound to ADPR and Ca^{2+}, the local region of S6 that includes I1045 and Q1053 tilts away from the central cavity, thereby dilating the lower gate to a similar radius as the selectivity filter, promoting channel-open probability (Fig. 5, C and D). This pore enlargement, however, is not sufficient to allow the passage of hydrated Ca^{2+} ions, which are ~4 Å in radius. Comparatively, the lower gate of the doubly bound state of *dr*TRPM2 is wider (fig. S10E). However, in this presumed open state, the selectivity filter of *dr*TRPM2 becomes the most constricted point in the ion conductive pathway (28), and its width is similar to that of the selectivity filter of *hs*TRPM2. Therefore, both *hs*TRPM2 and *dr*TRPM2 structures in complex with ADPR and Ca^{2+} may represent an intermediate state on the way to the fully open state; the latter may be quite transient, as shown by single-channel recordings (fig. S8).

Conformational changes at TRP H1 and the S6 gating helix accompany the widening of the lower gate to promote channel-opening probability. In a closed state, either apo or primed, TRP H1 connects to S6 via a continuous helix that bends at the junction (Fig. 5F). Upon Ca^{2+} binding to ADPR-primed TRPM2, the beginning part of TRP H1 and the ending part of S6 melt together into a loop, which likely releases the pull on S6 by TRP H1 and allows it to rotate and translate (Fig. 5, F and G), as also seen in the dfTRPM2 structure (28). Because TRP H1 directly binds to Ca^{2+}, we propose that it brings about Ca^{2+}-induced conformational changes at the S6 gating helix (Fig. 5, E to G). In this state, doubly bound to ADPR and Ca^{2+}, there is an additional contact between the melted S6-TRP connection and S6 of a neighboring subunit, which may stabilize the open conformation (Fig. 5H).

For some TRP channels, an α helix–to–π helix transition in a region of S6 has been proposed to cause gating (33, 34). For TRPM2 structures from the different species presented here and published previously (26, 28), the π-helix segment already exists in the closed conformation, suggesting that TRPM2 must be gated differently. Of note, many cation channels use the S4-S5 linker within the S1-S4 VSLD to cause a conformational change at the S6 gating helix (35). In hsTRPM2 and dfTRPM2 (28), TRP H1 sits adjacent to the S4-S5 linker, and it is possible that TRP H1 couples to S4-S5 to effect gating indirectly as well as through its direct connection to S6. Because TRP H1 consistently links to both the TM and the cytosolic domain through extensive interactions in available structures in the TRP family (fig. S11), we propose that the role of TRP H1 as an allosteric center to regulate gating, as revealed from the current study, may be more general than previously appreciated.

Discussion

Our cryo-EM structures of hsTRPM2 in the apo, ADPR-bound, and ADPR- and Ca^{2+}-bound states reveal conformational regulation of TRPM2 gating (Fig. 6 and Movie 1). In the apo state, the NUDT9H domain forms both intra- and intersubunit interactions, which may be important for locking TRPM2 in a closed state. Supporting this autoinhibition concept, small-molecule inhibitors for the related TRPM4 channel have been shown to bind at these interfaces (22, 23). Specifically, adenosine triphosphate (ATP) binding at the subunit interface has an inhibitory role in TRPM4 activity (22), and, although more complex, one of the decavanadate molecules also nestles at a subunit interface (23). In addition to sensing Ca^{2+} and ADPR, hsTRPM2 has been shown to sense body temperature to limit the fever response (11, 12). By contrast, dfTRPM2 lacks intersubunit interactions (28) and does not respond to heat or pH (36). We speculate that higher temperature, in the form of enhanced thermal motion, may overcome the intersubunit interactions in hsTRPM2 to modulate gating.

The apo conformation of TRPM2 is dramatically altered upon ADPR binding, with large domain rotation in MHR1/2 and local changes in MHR3, as well as disengagement of the intersubunit interaction. This effect of ADPR may allow the cytosolic domain of each subunit to freely rotate when Ca^{2+} binds at S2, S3, and TRP H1. In contrast to ADPR, the priming conformational changes by Ca^{2+} may be more subtle, as suggested by the lack of gross conformational differences between the apo state of hsTRPM2 and the Ca^{2+}-bound state of nvTRPM2 (fig. S12). The tilt of TRP H1 and melting at the S6-TRP junction, as

well as the proximity of the S4-S5 linker to TRP H1, may all help to twist the gating helix S6 to enhance the channel-opening probability. Because of its strategic location and coupling to both the TM and the cytosolic domain (fig. S11), TRP H1 appears to be especially important for gathering allosteric signals from various parts of the channel to effect gating, a hypothesis that may be further tested in multiple TRP channels. During the conformational transitions accompanying either priming or opening, the coiled coil formed by the pole helix remains unchanged, as if serving as a central spine to provide an anchor for movements at the periphery.

Intriguingly, the *dr*TRPM2 structure showed ADPR binding at MHR1/2 instead of at NUDT9H (28). Our experimental data demonstrate that this ADPR binding mode represents a true difference between *dr*TRPM2 and *hs*TRPM2, as NUDT9H of *dr*TRPM2 has affinity to ADPR in the millimolar range (fig. S5G), likely much higher than an inducible intracellular ADPR concentration, and mutations at MHR1/2 did not affect Ca^{2+} signaling by *hs*TRPM2 (fig. S5B). In this regard, previous studies showed that NUDT9H of *nv*TRPM2 degrades ADPR but plays no role in coactivation by ADPR and Ca^{2+} (37), whereas NUDT9H of *hs*TRPM2 binds ADPR to promote gating but does not have the ability to hydrolyze ADPR. Additional studies on species-specific aspects of TRPM2 structure and function are required to further tease out the complexity.

Materials and methods summary

Full-length *hs*TRPM2 with an N-terminal MBP tag was expressed in HEK293F cells and solubilized in 50 mM HEPES at pH 7.4, 150 mM NaCl, 2 mM TCEP, 2% glycerol, 1% LMNG, 0.1% CHS, and a protease inhibitor cocktail. TRPM2 was purified by amylose affinity resin followed by glycerol gradient and dialysis. For the cryo-EM study, 1 mg/ml TRPM2 was applied to grids and plunge-frozen using Vitrobot Mark IV. All the cryo-EM data were collected on a Titan Krios and processed using standard procedures.

Supplementary Material

Refer to Web version on PubMed Central for supplementary material.

ACKNOWLEDGMENTS

REFERENCES AND NOTES

1. Clapham DE, TRP channels as cellular sensors. Nature 426, 517–524 (2003). doi: 10.1038/ nature02196; [PubMed: 14654832]

2. Venkatachalam K, Montell C, TRP channels. Annu. Rev. Biochem 76, 387–417 (2007). doi: 10.1146/annurev.biochem.75.103004.142819; [PubMed: 17579562]

3. Julius D, TRP channels and pain. Annu. Rev. Cell Dev. Biol 29, 355–384 (2013). doi: 10.1146/annurev-cellbio-101011-155833; [PubMed: 24099085]

4. Tóth B, Iordanov I, Csanády L, Putative chanzyme activity of TRPM2 cation channel is unrelated to pore gating. Proc. Natl. Acad. Sci. U.S.A 111, 16949–16954 (2014). doi: 10.1073/pnas.1412449111; [PubMed: 25385633]

5. Iordanov I, Mihályi C, Tóth B, Csanády L, The proposed channel-enzyme transient receptor potential melastatin 2 does not possess ADP ribose hydrolase activity. eLife 5, e17600 (2016). doi: 10.7554/eLife.17600; [PubMed: 27383051]

6. Nagamine K et al., Molecular cloning of a novel putative Ca^{2+} channel protein (TRPC7) highly expressed in brain. Genomics 54, 124–131 (1998). doi: 10.1006/geno.1998.5551; [PubMed: 9806837]

7. Perraud AL et al., ADP-ribose gating of the calcium-permeable LTRPC2 channel revealed by Nudix motif homology. Nature 411, 595–599 (2001). doi: 10.1038/35079100; [PubMed: 11385575]

8. Sano Y et al., Immunocyte Ca^{2+} influx system mediated by LTRPC2. Science 293, 1327–1330 (2001). doi: 10.1126/science.1062473; [PubMed: 11509734]

9. Csanády L, Törocsik B, Four Ca^{2+} ions activate TRPM2 channels by binding in deep crevices near the pore but intracellularly of the gate. J. Gen. Physiol 133, 189–203 (2009). doi: 10.1085/jgp.200810109; [PubMed: 19171771]

10. Uchida K, Tominaga M, TRPM2 modulates insulin secretion in pancreatic β-cells. Islets 3, 209–211 (2011). doi: 10.4161/isl.3.4.16130; [PubMed: 21636972]

11. Song K et al., The TRPM2 channel is a hypothalamic heat sensor that limits fever and can drive hypothermia. Science 353, 1393–1398 (2016). doi: 10.1126/science.aaf7537; [PubMed: 27562954]

12. Tan CH, McNaughton PA, The TRPM2 ion channel is required for sensitivity to warmth. Nature 536, 460–463 (2016). doi: 10.1038/nature19074; [PubMed: 27533035]

13. Perraud AL et al., Accumulation of free ADP-ribose from mitochondria mediates oxidative stress-induced gating of TRPM2 cation channels. J. Biol. Chem 280, 6138–6148 (2005). doi: 10.1074/jbc.M411446200; [PubMed: 15561722]

14. Yamamoto S et al., TRPM2-mediated Ca^{2+} influx induces chemokine production in monocytes that aggravates inflammatory neutrophil infiltration. Nat. Med 14, 738–747 (2008). doi: 10.1038/nm1758; [PubMed: 18542050]

15. Knowles H et al., Transient receptor potential melastatin 2 (TRPM2) ion channel is required for innate immunity against Listeria monocytogenes. Proc. Natl. Acad. Sci. U.S.A 108, 11578–11583 (2011). doi: 10.1073/pnas.1010678108; [PubMed: 21709234]

16. Tripathi JK et al., Oxidant sensor cation channel TRPM2 regulates neutrophil extracellular trap formation and protects against pneumoseptic bacterial infection. FASEB J 10.1096/fj.201800605 (2018). doi: 10.1096/fj.201800605;

17. Shakerley NL, Chandrasekaran A, Trebak M, Miller BA, Melendez JA, Francisella tularensis catalase restricts immune function by impairing TRPM2 Channel activity. J. Biol. Chem 291, 3871–3881 (2016). doi: 10.1074/jbc.M115.706879; [PubMed: 26679996]

18. Zhong Z et al., TRPM2 links oxidative stress to NLRP3 inflammasome activation. Nat. Commun 4, 1611 (2013). doi: 10.1038/ncomms2608; [PubMed: 23511475]

19. Yamamoto S, Shimizu S, Significance of TRP channels in oxidative stress. Eur. J. Pharmacol 793, 109–111 (2016). doi: 10.1016/j.ejphar.2016.11.007; [PubMed: 27838397]

20. Ostapchenko VG et al., The transient receptor potential melastatin 2 (TRPM2) channel contributes to b-amyloid oligomer-related neurotoxicity and memory impairment. J. Neurosci 35, 15157–15169 (2015). doi: 10.1523/JNEUROSCI.4081-14.2015; [PubMed: 26558786]

21. Autzen HE et al., Structure of the human TRPM4 ion channel in a lipid nanodisc. Science 359, 228–232 (2018). doi: 10.1126/science.aar4510; [PubMed: 29217581]

22. Guo J et al., Structures of the calcium-activated, non-selective cation channel TRPM4. Nature 552, 205–209 (2017). [PubMed: 29211714]

23. Winkler PA, Huang Y, Sun W, Du J, Lü W, Electron cryo-microscopy structure of a human TRPM4 channel. Nature 552, 200–204 (2017). [PubMed: 29211723]

24. Duan J et al., Structure of full-length human TRPM4. Proc. Natl. Acad. Sci. U.S.A 115, 2377–2382 (2018). doi: 10.1073/pnas.1722038115; [PubMed: 29463718]

25. Yin Y et al., Structure of the cold- and menthol-sensing ion channel TRPM8. Science 359, 237–241 (2018). doi: 10.1126/science.aan4325; [PubMed: 29217583]

26. Zhang Z, Tóth B, Szollosi A, Chen J, Csanády L, Structure of a TRPM2 channel in complex with Ca^{2+} explains unique gating regulation. eLife 7, e36409 (2018). doi: 10.7554/eLife.36409; [PubMed: 29745897]

27. Duan J et al., Structure of the mammalian TRPM7, a magnesium channel required during embryonic development. Proc. Natl. Acad. Sci. U.S.A 115, E8201–E8210 (2018). doi: 10.1073/pnas.1810719115; [PubMed: 30108148]

28. Huang Y, Winkler PA, Sun W, Lü W, Du J, Architecture of the TRPM2 channel and its activation mechanism by ADP-ribose and calcium. Nature 562, 145–149 (2018). doi: 10.1038/s41586-018-0558-4; [PubMed: 30250252]

29. Shen BW, Perraud AL, Scharenberg A, Stoddard BL, The crystal structure and mutational analysis of human NUDT9. J. Mol. Biol 332, 385–398 (2003). doi: 10.1016/S0022-2836(03)00954-9; [PubMed: 12948489]

30. Yu P et al., Identification of the ADPR binding pocket in the NUDT9 homology domain of TRPM2. J. Gen. Physiol 149, 219–235 (2017). doi: 10.1085/jgp.201611675; [PubMed: 28108595]

31. Fliegert R et al., 2′-Deoxyadenosine 5′-diphosphoribose is an endogenous TRPM2 superagonist. Nat. Chem. Biol 13, 1036–1044 (2017). doi: 10.1038/nchembio.2415; [PubMed: 28671679]

32. Starkus J, Beck A, Fleig A, Penner R, Regulation of TRPM2 by extra- and intracellular calcium. J. Gen. Physiol 130, 427–440 (2007). doi: 10.1085/jgp.200709836; [PubMed: 17893195]

33. McGoldrick LL et al., Opening of the human epithelial calcium channel TRPV6. Nature 553, 233–237 (2018). doi: 10.1038/nature25182; [PubMed: 29258289]

34. Singh AK, McGoldrick LL, Sobolevsky AI, Structure and gating mechanism of the transient receptor potential channel TRPV3. Nat. Struct. Mol. Biol 25, 805–813 (2018). doi: 10.1038/s41594-018-0108-7; [PubMed: 30127359]

35. Catterall WA, Wisedchaisri G, Zheng N, The chemical basis for electrical signaling. Nat. Chem. Biol 13, 455–463 (2017). doi: 10.1038/nchembio.2353; [PubMed: 28406893]

36. Nam Tran H et al., Functional charaterization of zebrafish transient receptor potential melastatin 2. Biophys. J 114, 641A–642A (2018). doi: 10.1016/j.bpj.2017.11.3463 [PubMed: 29414710]

37. Kühn F, Kühn C, Lückhoff A, Different principles of ADP-ribose-mediated activation and opposite roles of the NUDT9 homology domain in the TRPM2 orthologs of man and sea anemone. Front. Physiol 8, 879 (2017). doi: 10.3389/fphys.2017.00879; [PubMed: 29163217]

38. Smart OS, Neduvelil JG, Wang X, Wallace BA, Sansom MS, HOLE: A program for the analysis of the pore dimensions of ion channel structural models. J. Mol. Graph 14, 354–360 (1996). doi: 10.1016/S0263-7855(97)00009-X; [PubMed: 9195488]

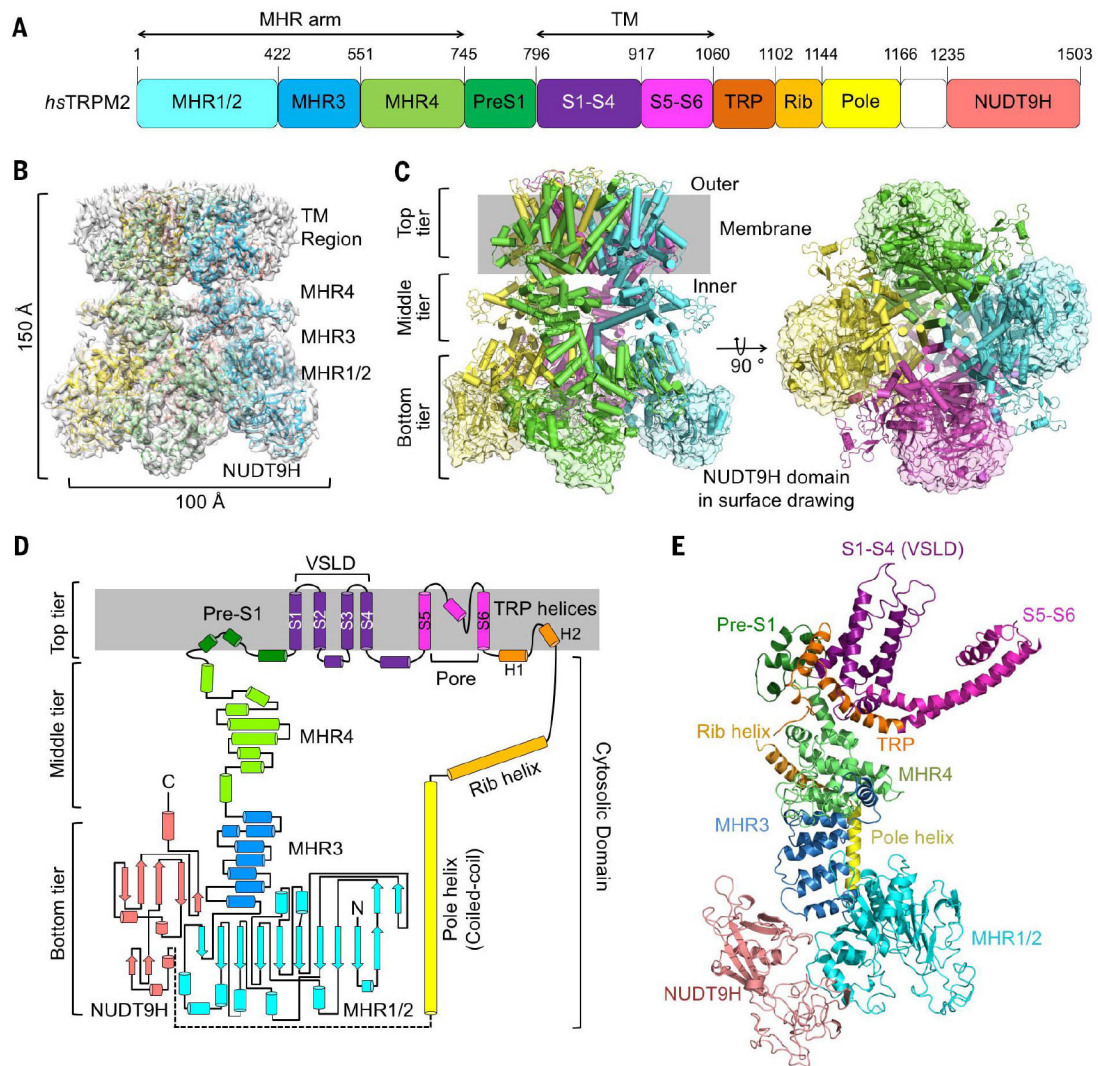**Fig. 1. Cryo-EM structure of *hs*TRPM2 in the apo, closed state.**
(**A**) Domain organization, with residue numbers indicated above. (**B**) Side view of the 3D cryo-EM density superimposed with the atomic model. Four subunits in the tetramer are colored in green, cyan, magenta, and yellow. The tetramer has estimated dimensions of 150 Å by 100 Å by 100 Å. (**C**) Ribbon diagrams with the subunits colored in green, cyan, magenta, and yellow and in two orthogonal views. The model is divided into three tiers, and the NUDT9H domain model is overlaid with a transparent surface representation. (**D**) Illustration of the major structural components and their spatial organization, shown in the same color scheme as in (A). (**E**) A ribbon diagram of a monomeric subunit, with domains labeled and colored according to the illustration in (D).
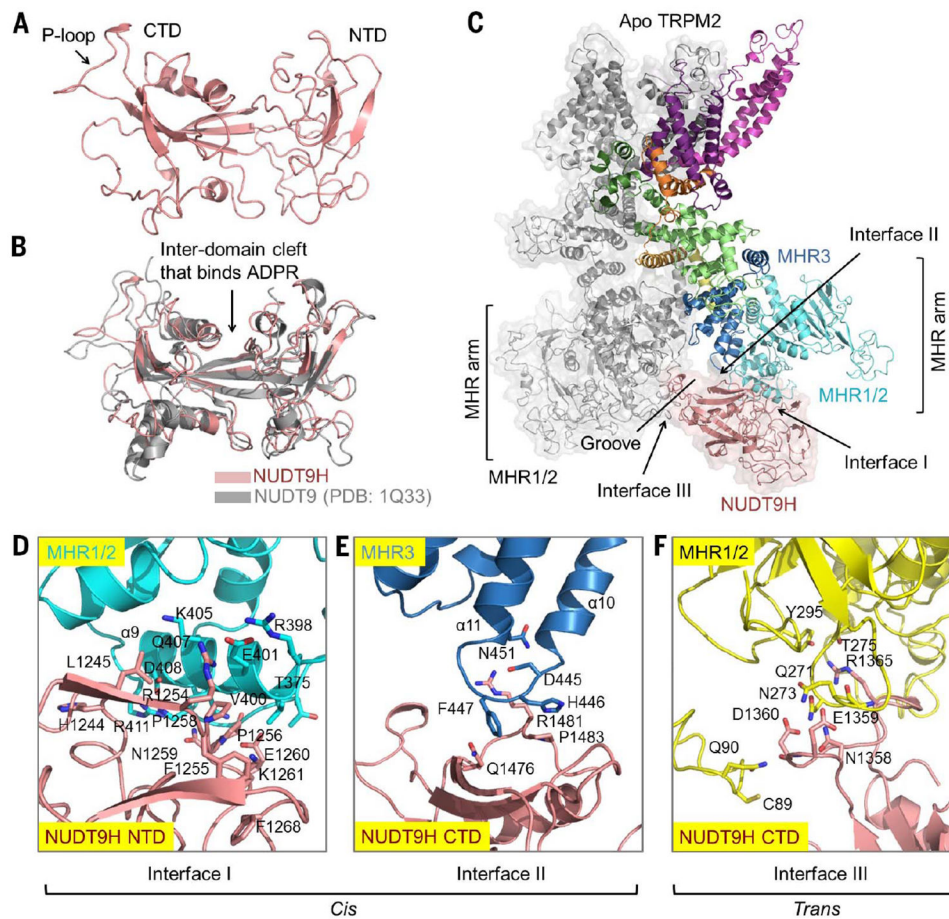
Fig. 2. NUDT9H and its interactions with the MHR1/2 and MHR3 domains.
(**A**) Structure of NUDT9H in a two-domain architecture. The location of the P loop is labeled. (**B**) Structural comparison between NUDT9H and human NUDT9 (PDB 1Q33) (29). (**C**) Three interfaces mediated by NUDT9H that contact in cis the MHR1/2 and MHR3 domains and in trans the MHR1/2 domain of a neighboring subunit. (**D** to **F**) Depiction of the three interfaces in detail. At interface I (D), the NUDT9H NTD closely contacts helix a9 from MHR1/2, forming charge-charge interactions between R1254 and E401, hydrogen bonds between N1259 and Q407/D408 and between E1260 and Q407, and hydrophobic interactions among P1256, P1258, V400, and K405 and between F1255 and V400. The NUDT9H CTD and the α10-α11 region of MHR3 establish interface II (E), in which R1481 and E476 form charge-charge interactions while Q1476, P1483, F447, and H446 form hydrophobic interactions. Interface III (F) features mostly hydrophilic interactions formed by the P loop of one subunit and MHR1/2 of a neighboring subunit, such as those between D1360 and Q90, between E1359/N1358 and Q271, and between N273 and R1365. Single-letter abbreviations for the amino acid residues are as follows: A, Ala; C, Cys; D, Asp; E, Glu; F, Phe; G, Gly; H, His; I, Ile; K, Lys; L, Leu; M, Met; N, Asn; P, Pro; Q, Gln; R, Arg; S, Ser; T, Thr; V, Val; W, Trp; and Y, Tyr.
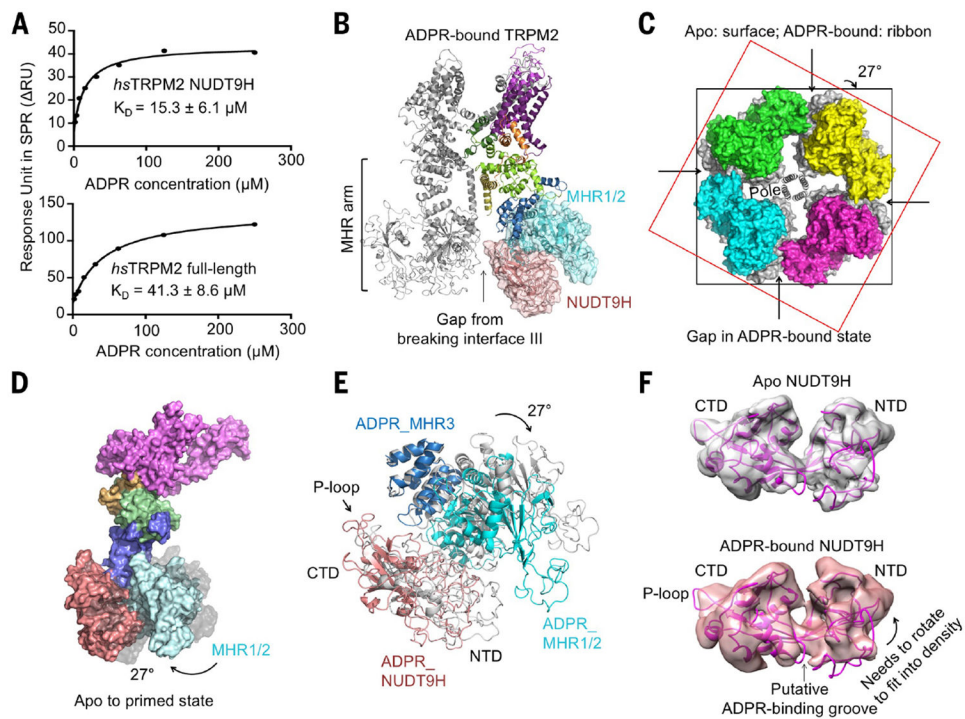
Fig. 3. TRPM2 priming by ADPR binding to NUDT9H.
(**A**) ADPR binding affinities to NUDT9H (top) and full-length TRPM2 (bottom), as measured by surface plasmon resonance (SPR). RU, change in response units; K_D, dissociation constant. (**B**) A ribbon diagram of ADPR-bound TRPM2 shown as a dimer, with one subunit in domain colors and the other subunit in gray. Disruption of the intersubunit interaction is indicated. (**C**) Top view of overlaid tetramers of TRPM2 in ADPR-bound state (colored surface) and in apo state (gray surface), showing a 27° rotation between subunits in the two states. Two squares help to indicate the rotation. (**D**) Side view of one subunit in surface representation, showing the conformational changes of TRPM2 from the apo state (gray) to the ADPR-bound state (colored). (**E**) Overlaid side-view ribbon diagrams, showing the rotation of NUDT9H, MHR1/2, and MHR3 domains from the apo state (gray) to the ADPR-bound state (colored). (**F**) Comparison of NUDT9H densities in the apo state (gray) and the ADPR-bound state (salmon). The NUDT9H model from the apo state (magenta) is fitted into the ADPR-bound state density as a rigid body. The P-loop region and the NTD that needs to be rotated are indicated.
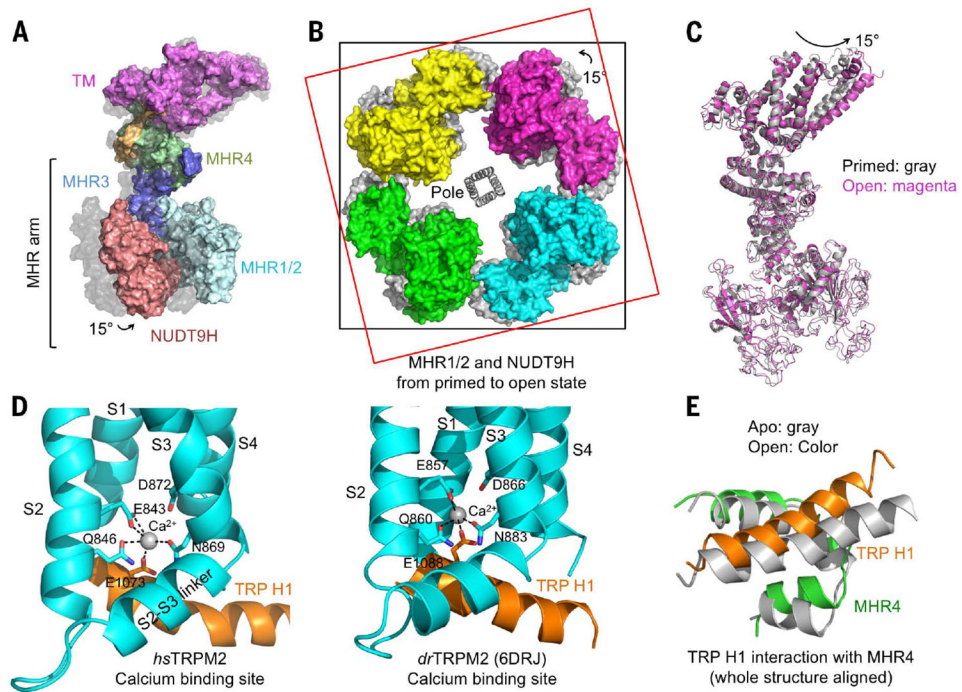
Fig. 4. Global conformational changes of *hs*TRPM2 during its opening.
(**A**) Side view of one subunit in surface representation, showing a 15° rotation from the primed state (gray surface) to the open state (colored surface). The entire MHR arm moves. (**B**) Top view of overlaid tetramers in the open state (colored surface) and the primed state (gray surface). Two squares help to indicate the rotation. (**C**) Superimposed TRPM2 structures in the primed (gray) and open (magenta) states. (**D**) Coordination of Ca^{2+} by residues in TRP H1, S2, and S3 in both *hs*TRPM2 and *dr*TRPM2 (PDB 6DRJ) (28). (**E**) TRP H1 and MHR4 are positioned in close proximity via direct interactions, shown as a global superposition between the apo (gray) and open (colored) states. TRP H1 tilts as a consequence of Ca^{2+} binding, establishing a molecular coupling between TRP H1 and the cytosolic domain.
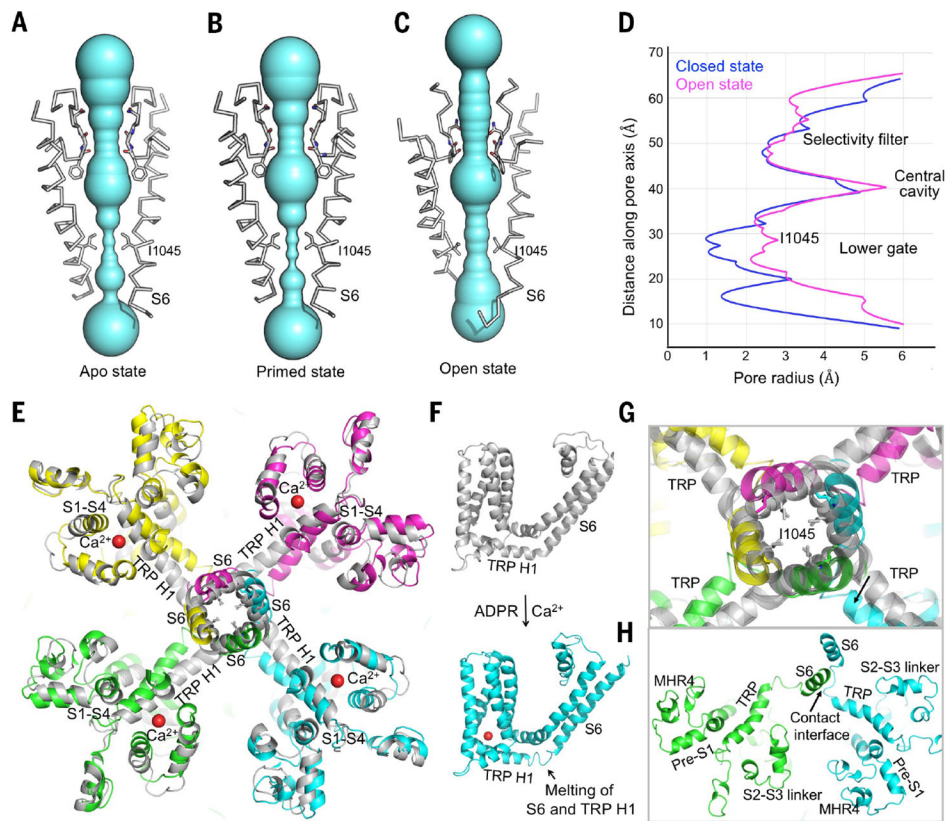
Fig. 5.
Conformational changes of the ion permeation pore. (**A** to **C**) Pore-forming domain of TRPM2 in apo (A), ADPR-bound (B), and open (C) states, with key residues lining the pore shown as sticks. The pores are shown as space-filling models and were calculated using the HOLE program (38). (**D**) Pore radii of apo (blue) and open (magenta) states along the pore axis, calculated as in (A) to (C). (**E**) Comparison of the TM region in apo (gray) and open (colored) states. Bound Ca^{2+}, S6, TRP H1, and S1-S4 are labeled. (**F**) TM region of the apo (gray) and open (cyan) states, showing a partial melting of S6 and TRP H1 in the open state. (**G**) Enlarged view of the conformational change near residue I1045 at the lower gate. (**H**) The open state conformation may be stabilized by the trans interaction between S6 and the melted S6-TRP helix loop.
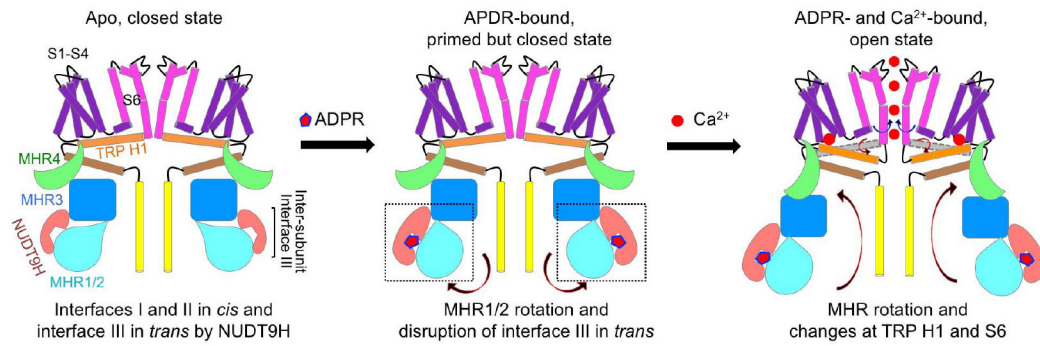
Fig. 6. A model for *hs*TRPM2 gating.

In the apo state (left), the channel is in a closed conformation with S6 (magenta) forming the lower gate and NUDT9H (pink) interacting with MHR1/2 (cyan) and MHR3 (blue) in cis and MHR1/2 from a neighboring subunit in trans. Upon ADPR binding (middle), rotation of MHR1/2 and disengagement of the trans interaction prime the channel for opening. Binding of Ca^{2+} directly engages S2 and S3 helices (purple) and TRP H1 (orange), leading to a tilt at TRP H1 and partial melting at the S6-TRP junction to trigger S6 rotation and channel opening. In the open conformation cartoon (right), the gray helix represents TRP H1 in a closed state and is shown for comparison with TRP H1 in the open state (orange). Arrows indicate conformational transitions.
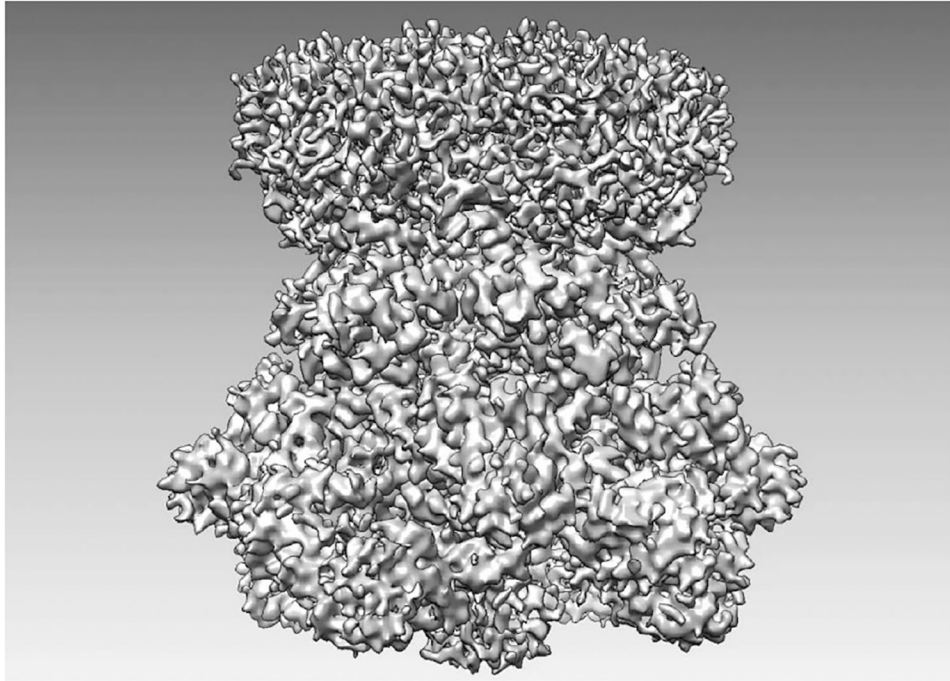
Movie 1.
Conformational changes of *hs*TRPM2 during channel opening.